Hindawi Publishing Corporation
Advances in Civil Engineering
Volume 2012, Article ID 452987, 9 pages
doi:10.1155/2012/452987

Research Article

Behavior of FRP Link Slabs in Jointless Bridge Decks

Aziz Saber and Ashok Reddy Aleti

Department of Civil Engineering, Louisiana Tech University, 600 West Arizona Avenue, Ruston, LA 71272, USA

Correspondence should be addressed to Aziz Saber, saber@latech.edu

Received 4 January 2012; Revised 23 March 2012; Accepted 24 March 2012

Academic Editor: Sami W. Tabsh

The paper investigated the use of fiberglass-reinforced plastic (FRP) grid for reinforcement in link slabs for jointless bridge decks. The design concept of link slab was examined based on the ductility of the fiberglass-reinforced plastic grid to accommodate bridge deck deformations. The implementation of hybrid simulation assisted in combining the experimental results and the theoretical work. The numerical analyses and the experimental work investigated the behavior of the link slab and confirmed its feasibility. The results indicated that the technique would allow simultaneous achievement of structural need, lower flexural stiffness of the link slab approaching the behavior of a hinge, and sustainability need of the link slab. The outcome of the study supports the contention that jointless concrete bridge decks may be designed and constructed with fiberglass-reinforced plastic grid link slabs. This concept would also provide a solution to a number of deterioration problems associated with bridge deck joints and can be used during new construction of bridge decks. The federal highway administration provided funds to Louisiana Department of Transportation through the innovative bridge research and development program to implement the use of FRP grid as link slab.

1. Introduction

Thousands of bridges in the United States are constructed as simple spans. The bridges require the use of expansion joints over piers. The joints create short-term and long-term problems. Some examples of these problems are leaks through the joints deteriorating the supporting girders and the piers and debris accumulating in the joints which prevents them from functioning properly. These problems lead to massive direct and indirect costs (Saber et al. [1, 2]). Therefore there is a need for reducing or eliminating expansion joints in bridge decks. The objectives of this study are to develop and evaluate a new technique using advancement in materials and current technology. An innovative system is proposed for this study. The new system replaces expansion joints with a link slab. The link slab joins decks of adjacent spans without imposing any continuity in the bridge girders. The link slab is subjected to tensile forces and stresses due to the negative moment developed at the joint. Fiberglass-reinforced plastic (FRP) reinforcement is used to carry the tension forces (Saber [3]) and its corrosion resistance.

The most common type of reinforcement used in bridge construction is steel rods. The deterioration of steel caused by corrosion has been plaguing these structures across the nation, decreasing their service life, and increasing the cost of repair and maintenance. Many investigations were conducted to resolve the problems associated with corrosion by such methods as decreasing the porosity of concrete, coating steel bars with a protective outer layer, and increasing the reinforcement cover. But these methods only extend the time it takes for corrosion to take place.

For more than three decades, researchers have investigated the use of FRP (fiberglass reinforced polymers) as an alternate to steel reinforcement in concrete structures. In recent years, the use of FRP rods for structural applications has been gaining acceptance around the world. Recently FRP grids have been used for reinforcement of concretes beams and slabs (Dutta et al. [4]). A grid is a latticework of rigid, interconnecting ribs in two, three, or four groups and directions. Such grid reinforcement enhances the energy absorption capability and the overall ductility of the structure is improved. This leads to an increase in the ultimate load carrying capacity of concrete beams and slabs. When the opening of grids is filled with concrete, the combined structure derives its shear rigidity from the concrete filler and the concrete prevents the ribs from buckling. FRP composite

grids provide a mechanical anchorage within the concrete due to the interlocking elements (cross-ribs), and therefore no bond is necessary for proper load transfer.

Although there have been a number of studies on the use of FRP-grid-reinforced concrete beams or slabs, there is currently a lack of information on the use of FRP-grid-reinforced concrete link slabs for the replacement of expansion joint. Because the link slab will be subjected to a negative bending moment and thermal stress, it is expected that the design and performance will be different from conventional beams or slabs, which is primarily subjected to a positive bending moment and transverse shear force. Therefore, there is a need to conduct experimental testing and theoretical modeling analysis of FRP-grid-reinforced concrete link slabs for the replacement of expansion joints.

2. Experimental Work

A test program was conducted to determine the behavior and strength of jointless bridge decks under static loading. The jointless decks could be achieved by replacing expansion joints with a link slab that could join bridge decks of adjacent spans without imposing any continuity in the bridge girders. The link slab would be subjected to tensile forces due to negative moment developed at the location of the joint. The link slab panel was cut into beam specimens to determine the strength of the link slab against tensile forces. The test program included specimens with two layers of FRP grids. The specimens were tested under the same support conditions. Loads, deflections, strains, and load carrying capacity were measured for each test specimen.

2.1. Test Specimens. The specimens were designed as per ASTM C 78, ACI 318, and ACI 440 guidelines, [5, 6]. Since there was no design code for FRP-grid-reinforced concrete beams, the existing design equations in ACI 440 for FRP rebar-reinforced concrete beams were modified and used. The cross section of the specimens was rectangular in shape with a width of 300 mm (1 ft), 200 mm (8 in) deep, and 2.4 m (8 ft) long. The FRP grids were placed in the center 1.2 m (4 ft) of the beams. The first specimen, beam 1, contained two layers of FRP grid; each is 25 mm (1 in) deep, 1.2 m (4 ft) long, and 225 mm (9 in) wide. The clear spacing between the two FRP grids was 25 mm (1 in). Shear reinforcement was not provided to the beams since the depth of the beam did not exceed the requirements of ACI 318 [5]. Also, three number 13 (number 4) rebars were placed in the specimens for handling. The dimensions and cross-section details of the beam 1 were shown in Figures 1 and 2, respectively.

The second beam, beam 2, contained two layers of 31 mm (1.25 in) deep FRP grids, 1200 mm (4 ft) long, and 225 mm (9 in) wide. The dimensions and cross-section details of beam 2 were similar to beam 1, as shown in Figure 3. The two rectangular beams were cast from the batch delivered by a ready mix truck to the Structural and Materials Laboratory at Louisiana Tech University. To simulate field conditions, the beams were cured in dry air conditions for 28 days before they were tested.

The specimens were tested under the same set-up as shown in Figure 1. The applied loads and reactions were symmetrical with respect to the center of the beam. The specimen was placed on a high reaction stand of a stiffened steel section. At each reaction point, a roller support was placed between the specimen and the steel section. Load was applied by an MTS hydraulic jack at load points. A steel section was used between the hydraulic jack and the beam specimen to apply the load equally at the load locations. At the load points, roller supports were provided to disperse the load from the steel section to the specimen. The jack was activated by a single automatic MTS electric pump.

2.2. Instrumentation Plan. The instrumentation used for the testing of each beam included a deflectometer, a twenty-four channel data acquisition system, and 50 mm (2 in) long strain gages installed at locations on the FRP grids where the shear forces and bending moments were high. The strain gages were installed on the outer surface along the longitudinal direction. The top grid was designated as layer 1 and the bottom grid was designated as layer 2. Layer 1 strain gages were designated as L1G1 through L1G8 from left end to the right end of the grid. Similarly, layer 2 strain gages were designated as L2G1 through L2G8 from left end to the right end of the grid. The deflection of each beam was measured during the test by a deflectometer placed at the midspan of the beam.

2.3. Test Procedure. A four-point bending test was conducted, and the test load was applied in such a way that a negative bending moment was produced in the beam at the FRP grid locations. The beams were loaded continuously at a constant rate of 8.9 kN/min (2 kip/min) until failure. The four-point bending tests were conducted using the MTS machine. The data collection system stored the strain and load data for every quarter second. For each load increment, data for the FRP strains and loads were collected. The applied loads and corresponding deflections at midspan for each beam were measured during the tests.

2.4. Material Characteristics. The concrete mix constituents were shown in Table 4. The concrete cylinders were cast from the same batch delivered by a local ready mix truck to the Structural and Materials Laboratory at Louisiana Tech University.

The concrete cylinders 100 × 200 mm (4 × 8 in) were cured in accordance with ASTM C511, and the compressive strength was determined in accordance with ASTM C39. The average compressive strength of three cylinders was recorded for each test day and the strength development over time is shown in Figure 4. When the beam specimens were tested at 28 days, the compressive strength of the concrete was 36.4 MPa (5277 psi).

The material properties of FRP grid were obtained from the manufacturer (Fibergrate, Composite Structures) and were listed in Table 1.

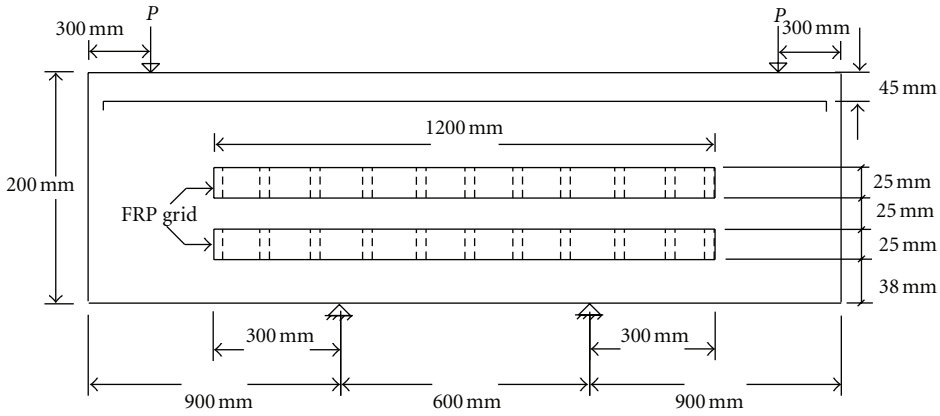

Figure 1: Beam 1 dimensions (not to scale).

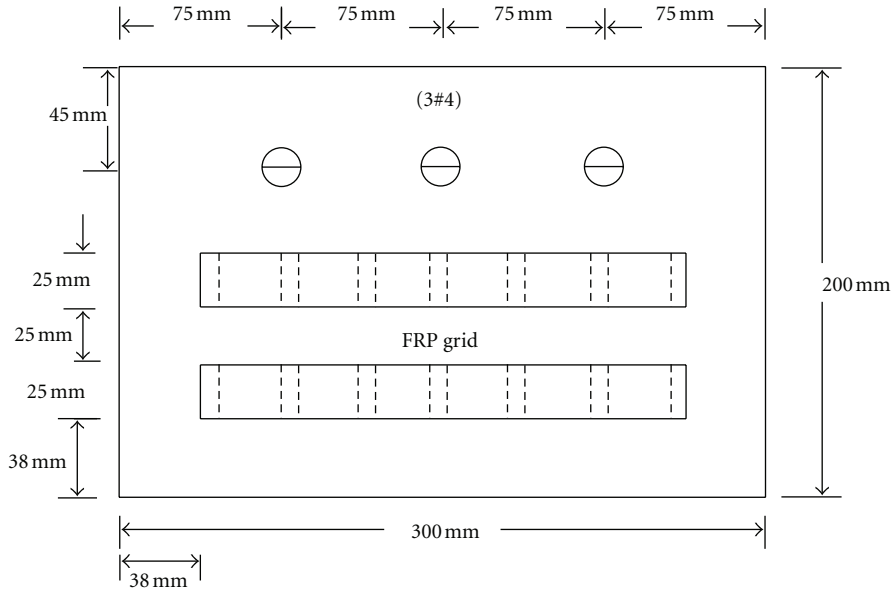

Figure 2: Beam 1 cross-section details.

Table 1: Concrete mix proportions.

Cement	222 kg/m^3 (489 lb/yd^3)
Fly Ash	55 kg/m^3 (122 lb/yd^3)
Coarse aggregate pea gravel	849 kg/m^3 (1870 lb/yd^3)
Natural Sand	602 kg/m^3 (1325 lb/yd^3)
Admixture (900 P0Y-5)	0.53 liter/m^3 (18 Oz/yd^3)
Air content	0.05
Slump	125 mm (5 inch)
Water	112 liter/m^3 (29.5 gal/yd^3)

2.5. Experimental Results. The specimens were designed to be underreinforced so that large strains in FRP grids preceded the crushing of the concrete in compression. The discussion will be given on strain responses up to failure, the overall load/deflection, and the mode of failure of the specimens. The beams were designed to have ductile failure at the ultimate load, as would be the case for existing bridge decks in service. The flexural cracks formed in the constant moment region extended vertically and became wider and then progressed towards the load points in a diagonal fashion. The beam then collapsed as shown in Figure 5.

2.6. Beam 1 Failure. The longitudinal strains in the FRP grids due to the applied loads were recorded. The strain data in the cantilever section indicated that the longitudinal strain distribution followed the bending moment diagram. In Figures 6 and 7, the data obtained from the strain gages indicated that at higher loads the longitudinal strains in the shear spans increased above those of a linear variation. This showed that strains were not proportional to the applied moment at these locations. At ultimate conditions, the axial

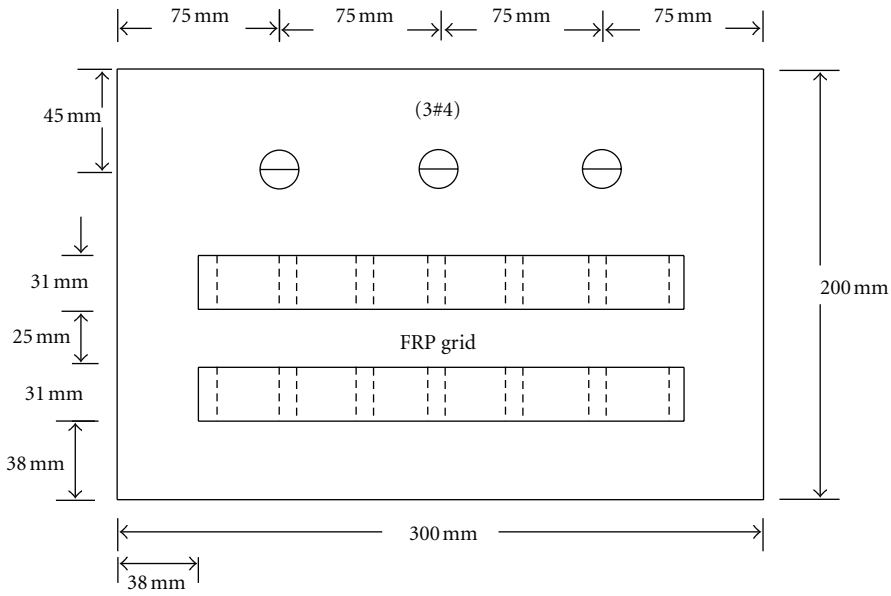

Figure 3: Beam 2 cross-section details.

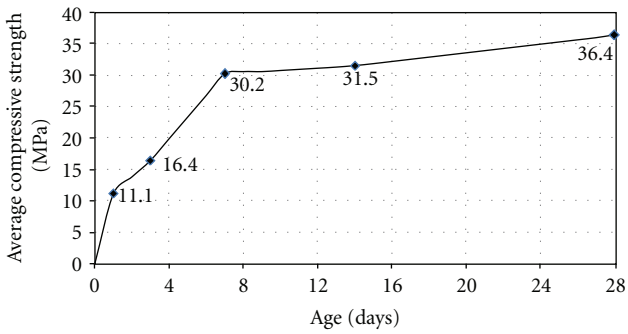

Figure 4: Concrete average compressive strength.

Figure 5: Beam 2 at collapse.

strain in the FRP grid varied linearly along the end of the FRP gird and at the point of load. Based on the previous discussion, it was concluded that the bond between the FRP grid and concrete is uniform. Moreover, the data in Figures 6 and 7 indicated that the variations in the strain with the load at the beam center were slightly higher than those close to the load point, but the two curves were of similar form. As the applied load increased, the rate of change in the strains in the shear span was higher than that in the constant moment region. The higher rates demonstrated the initiation and progress of cracking in the region close to the support. The high level of strains in the shear span explained the flexural/shear cracking in the collapse mechanism for the beam.

Table 2: FRP grid material properties provided by manufacturer.

Material characteristics	Value
Tensile stress, LW	207 MPa (30,000 psi)
Tensile modulus, LW	17.2 GPa (2.5×10^6 psi)
Compressive stress, LW	207 MPa (30,000 psi)
Compressive modulus, LW	17.2 GPa (2.5×10^6 psi)
Flexural stress, LW	207 MPa (30,000 psi)
Flexural modulus, LW	12.4 GPa (1.8×10^6 psi)
Shear modulus	3.1 GPa (0.45×10^6 psi)
Short beam shear	31 MPa (4,500 psi)
Punch shear	68.9 MPa (10,000 psi)
Bearing stress, LW	207 MPa (30,000 psi)
Area of 1 inch deep FRP per 9 inch width per layer	894 mm^2 (1.43 in^2)
Area of 1.25 inch deep FRP per 9 inch width per layer	1112 mm^2 (1.78 in^2)

2.7. Strains in Beam 1 Layer 1. A total of eight strain gages were installed to monitor the strain distribution. The strains measured were tensile strains in all of the gages

Table 3: Maximum flexural stresses for bottom elements for bridge girders.

Girder number	Open joint bridge (OJB) maximum flexural stress (MPa)	Link slab bridge (LSB) maximum flexural stress (MPa)	Percentage of decrease in girder stresses due to link slab
S1G1	2.13	1.75	18%
S1G2	2.55	2.07	19%
S1G3	2.53	2.12	16%
S1G4	2.16	1.69	22%
S2G1	0.82	0.54	34%
S2G2	0.82	0.55	33%
S2G3	0.83	0.57	32%
S2G4	0.80	0.54	32%
S3G1	0.63	0.56	12%
S3G2	0.65	0.59	10%
S3G3	0.65	0.59	9%
S3G4	0.65	0.56	14%

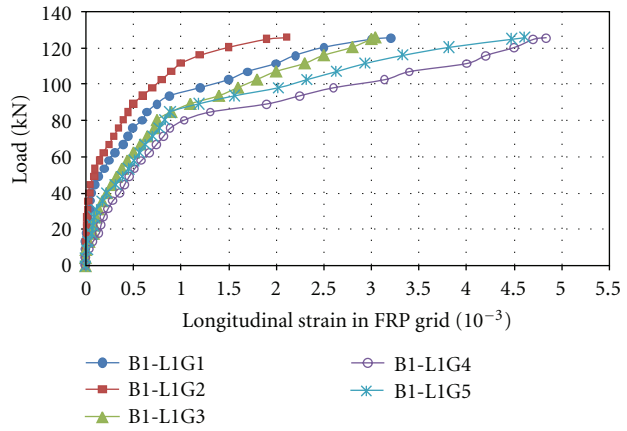

Figure 6: Load/strain along FRP grid for layer 1 in beam 1.

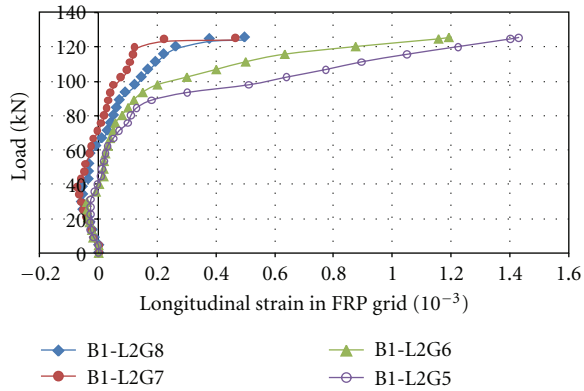

Figure 7: Load/strain along FRP grid for layer 2 in beam 1.

at different applied loads for the ultimate load test. These measurements indicated that the grid was in tension. Among all the gages, maximum tensile strain was found in gage 4 (B1-L1G4), which was located just right of the left support. The maximum strain was 4.8 milli strains at the ultimate load of 125.5 kN (28.2 kips). The tensile modulus of the grid was 17.2 GPa (2.5×10^3 ksi). Therefore, the tensile stress corresponding to maximum tensile strain was 82.7 MPa (12.0 ksi) which is 40% of the maximum tensile stress recommended by the manufacturer, as shown in Table 1. The load-strain relationship was linear up to the load level of 75.6 kN (17 kip) when the beam began to yield. The load-strain distribution of gage 5 in layer 1 (B1-L1G5) located at the center of grid and beam indicated that the changes in the strains were low up to the load level of 84.6 kN (19 kip), and after that, change in strains were higher until the ultimate load was reached. The strain distribution for layer 1 of beam 1 indicated that as the applied load increases towards its maximum value, the distribution of strain in the FRP grid became unsymmetrical.

2.8. Strains in Beam 1 Layer 2. The strains measured were compressive strains in all the gages up to an applied load of 40 kN (9 kips). Then the measured strains were changed to tensile strains for the ultimate load test. These measurements indicated that the grid was in compression until the applied load reached a value of 40 kN (9 kip); then the grid was in tension. Among all the gages, the maximum compressive strain was found in gage 7 (B1-L2G7) located at 1.65 m (66 in) from the left end of the beam at an applied load of 40 kN (9 kips). The load-strain distribution of gage 7 in layer 2 (B1-L2G7) indicated that the maximum compressive strain was −0.074 millistrains. The compressive modulus of the grid was 17.2 GPa (2.5×10^3 ksi). Therefore, the compressive stress corresponding to maximum compressive strain was 1.24 MPa (0.18 ksi) which is 0.6% of the maximum compressive stress recommended by the manufacturer. The maximum tensile strain was found in gage 4 (B1-L2G4) which was located at just right to the left support. The maximum strain was 1.6 millistrains at the ultimate load 125.5 kN (28.2 kips). The tensile modulus of the grid was 17.2 GPa (2.5×10^3 ksi). Therefore, the

tensile stress corresponding to maximum tensile strain was 27.4 MPa (3.98 ksi) which is 13.3% of the maximum tensile stress. The strain distribution for layer 1 of beam 2 indicated that as the applied load increased towards its maximum value, the distribution of strain in the FRP grid became unsymmetrical.

2.9. Beam 2 Failure. The same discussion presented previously applies to the behavior for beam 2 with two 31 mm (1.25 in) FRP grids. The strain distribution in the FRP grid in layer 1 of the specimen beam 2 is shown in Figure 8.

2.10. Strains in Beam 2 Layer 1. A total of eight strain gages were installed to monitor the strain distribution. The strains measured were tensile strains in all the gages at different applied loads for the ultimate load test. These measurements indicated that the grid was in tension. Among all the gages, maximum tensile strain was found in gage 4 (B2-L1G4), which was located at just right to the left support. The maximum strain was 4.0 millistrains at the ultimate load of 113.9 kN (25.6 kips). The tensile modulus of the grid was 17.2 GPa (2.5×10^3 ksi). Therefore, the tensile stress corresponding to maximum tensile strain was 69.6 MPa (10.1 ksi) which is 34% of the maximum tensile stress recommended by the manufacturer. The load-strain distribution of gage 5 in layer 1 (B2-L1G5) located at the center of grid and beam indicated that at higher loads, strain varied linearly with the applied loads.

2.11. Strains in Beam 2 Layer 2. The strains measured were compressive strains in all eight gages up to an applied load of 62.3 kN (14 kips); after that, the measured strains were changed to tensile strains for the ultimate load test. These measurements indicated that the grid was in compression till the applied load reached a value of 62.3 kN (14 kips); then the grid was in tension. Among all the gages, the maximum compressive strain was found in gage 7 (B2-L2G7) located at right end of the grid at an applied load of 31.2 kN (7 kips). The load-strain distribution of gage 7 in layer 2 (B2-L2G7) indicated that the maximum compressive strain was −0.058 millistrains. The compressive modulus of the grid was 17.2 GPa (2.5×10^3 ksi). Therefore, the compressive stress corresponding to maximum compressive strain was 1 MPa (0.15 ksi) which is 0.5% of the maximum compressive stress recommended by the manufacturer. The maximum tensile strain was also found in gage 7 (B2-L2G7). The maximum strain was 0.21 millistrains at the ultimate load 114 kN (25.6 kips). The tensile modulus of the grid was 2.5×10^3 ksi. Therefore, the tensile stress corresponding to maximum tensile strain was 3.7 MPa (0.53 ksi) which is 1.8% of the maximum tensile stress.

2.12. Load-Deflection Behavior. All specimens were tested in a four-point bending configuration. The ultimate loads and corresponding deflections for both beams were measured during the tests. The load carrying capacity of the beam 1 was 125.5 kN (28.2 kips) and that for beam 2 was 114 kN (25.6 kips). The deflection of each beam at collapse was

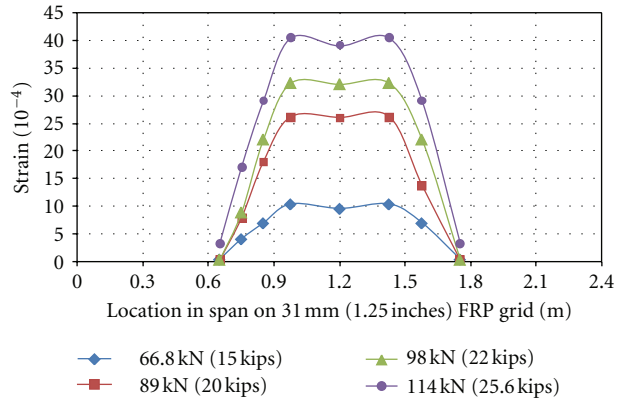

Figure 8: Longitudinal strain along FRP grid for layer 1 in beam 2.

substantial (L/240) accompanied by excessive cracking. The load deflection response of the specimens exhibited three regions of behavior. At low applied loads the stiffness of the reinforced concrete beam was relatively high, indicating that the concrete behaved in a linear elastic manner. As the load increased, the bending stress in the extreme fibers increased until the tensile strength at the top of the section of the concrete was reached. This caused flexural cracks to form, first in the constant moment region, then through the beam cantilever section. As the flexural cracks developed in the span, the member stiffness was reduced and the response after the cracking load was approximately linear due to the postcracking stiffness. After the concrete in the tension zone cracked, the FRP grid carried the tensile forces due to applied loads. As the applied load increased, the tensile stress increased the, beam stiffness was decreasing due to the loss of material stiffness, and the ability of the section to support the tensile stress was reduced. The yield plateau in the slope-deflection curve for beam 2 was longer than that of beam 1, which indicated that beam 2 was more ductile than beam 1, even though the areas of the FRP grids in beam 2 were greater than beam 1.

3. Theoretical Work

In this study, finite element models are developed to investigate the behavior of the bridge with link slabs. Two models are considered, one with open joints and another with the joints closed over the supports. The results of the models are compared and used to evaluate the structural behavior of the FRP-grid-reinforced link slab.

3.1. Bridge Model Description. The bridge models were developed using the software ANSYS. A typical three-span bridge was considered. In each span, four AASHTO Type III girders, end and intermediate diaphragms were modeled. The dimensions of the deck in the z-axis were 18 m (60 ft) long, 9 m (30 ft) wide in the x-axis, and 200 mm (8 in) thick in the y-axis. A gap of 25 mm (1 in) and 150 mm (6 in) was considered between two adjacent decks (open joint) and

two girders in adjacent spans, respectively. The center-to-center distance between adjacent girders in a span was 2.6 m (104 in). The end diaphragms were provided between two adjacent girders, from the middepth of girder to the bottom of the top flange. The intermediate diaphragms were placed from the top of bottom flange to the bottom of the top flange (Saber et al. [7]) The thickness of the intermediate and end diaphragms was 175 mm (7 in). The link slab was modeled for a distance of 600 mm (2 ft) at both adjacent ends of the open joint. The link slab length was based on the theoretical studies which showed that the load-deflection behavior of the structure would not be affected by a debonding length of up to 5% of the girder span length (Zia et al. [8]). The girders were restrained at supports and both extreme ends of the decks were restrained in x, y, and z directions (translations). The HL-93 loads were applied to the bridge models in such a way that they produced maximum negative moment and tensile force in the link slab.

3.2. Elements Used in Modeling. The FRP layers were meshed using SOLID46 element and material properties (Modulus of elasticity, Poisson's ratio, and density) were assigned during the process. The element edge length was 150 mm (6 in). A small size element was chosen because the depth of FRP was just 25 mm (1 in). The bridge decks and diaphragms were meshed using SOLID65 element and material properties (Modulus of elasticity, Poisson's ratio, and density) were assigned during the process. The element edge length of concrete element was 600 mm (24 in). The mesh was refined twice at the girder supports to restrain the girders properly over the piers (Saber et al. [9]).

3.3. Boundary Conditions and Loading System. In the model, the interface area between girders and substructure was restrained in the x and y directions (translations). Both extreme ends of the decks (area along the depth) were restrained in the x, y, and z directions (translations). LRFD Bridge Design [10] load combinations were considered, and the corresponding load factors were applied to the model. The vehicular live load and the live load surcharge were applied on the bridge. The truck load was applied to produce maximum negative moments in the link slab.

3.4. Comparison between Open Joint Bridge and Link Slab Bridge. The details for the finite element models are shown in Figure 9. The four girders in the first span of the bridge were designated as S1G1, S1G2, S1G3, and S1G4. Similarly, girders in the second span of the bridge were designated as S2G1, S2G2, S2G3, and S2G4 and girders in the third span of the bridge were designated as S3G1, S3G2, S3G3, and S3G4. Among all the girders, the maximum flexural stresses (tensile) were found in the second girder of the first span.

3.5. Girder Stresses

3.5.1. Span 1. The flexural stresses (tensile) for the bottom elements along the length of the second girder in the first span for the two bridge models were shown in Figure 10.

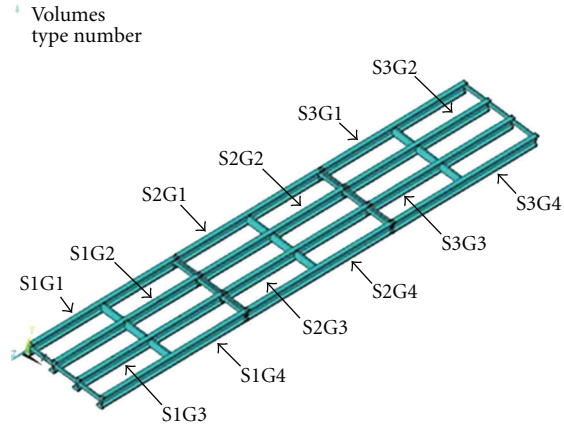

Figure 9: Model with the girders.

The flexural stresses were higher in the open joint bridge than those in the link slab bridge at most of the locations. A maximum flexural stress difference of 1 MPa (150 psi) was observed between the two girders, at a distance of 14.9 m (49 ft-8 in) from the left support. The flexural stresses were almost the same for a length of 6 m (20 ft) from the left support for both cases, but after that, the stresses in the open joint bridge were much higher. It can be inferred from the figure that the continuity in the decks reduces the flexural stresses in the girders.

3.5.2. Span 2. The flexural stresses (tensile) for the bottom elements along the length of the second girder in the second span for two bridge models were shown in Figure 11. The flexural stresses were higher in the open joint bridge than those in the link slab bridge at all locations. A maximum flexural stress difference of 0.28 MPa (40 psi) was observed between two girders, at a distance of 13.1 m (43 ft-9 in) from the left support.

3.5.3. Span 3. The flexural stresses (tensile) for the bottom elements along the length of the second girder in the third span for two bridge models were shown in Figure 12. A maximum flexural stress difference of 0.21 MPa (31 psi) was observed between two girders, at a distance of 3.7 m (12 ft-4 in) from the left support. The flexural stresses were higher in the open joint bridge up to 12 m (40 ft) from the left support and after that the flexural stresses were high in the link slab bridge.

3.6. Maximum Flexural Stresses in Girders. The maximum flexural stresses in the twelve girders of the open joint bridge, the link slab bridge, and the percentage change in stresses of the open joint bridge compared with link slab bridge were shown in Table 2. The stresses were higher in girders of the open joint bridge. The maximum decrease was 34% found in the girders of span 2 of the bridge, and the minimum decrease was 9% found in span 3. The maximum effects in span 1 where truck load was applied were in the range of 16% to 22%.

Table 4: Stresses in link slabs at the top and the bottom of bridge deck.

Results	Link slab 1 stress (MPa)		link slab 2 stress (MPa)	
Transverse stress (S_x)	Max.	0.53	Max.	0.23
	Min.	−0.09	Min.	−0.04
Longitudinal stress (S_z)	Max.	2.29	Max.	1.05
	Min.	−1.01	Min.	−0.20
Shear stress (S_{yz})	Max.	0.05	Max.	0.07
	Min.	−0.03	Min.	−0.01

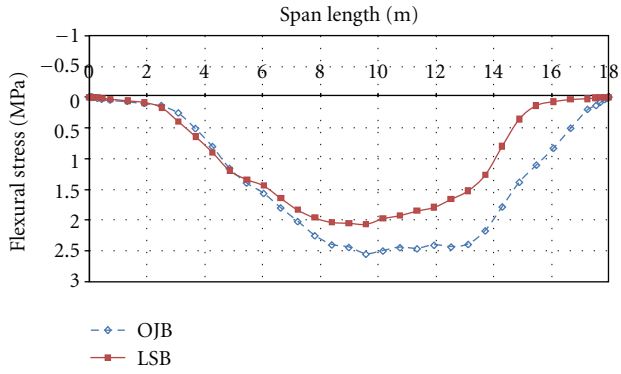

Figure 10: Flexural stresses for bottom elements of 2nd girder in 1st span (S1G2).

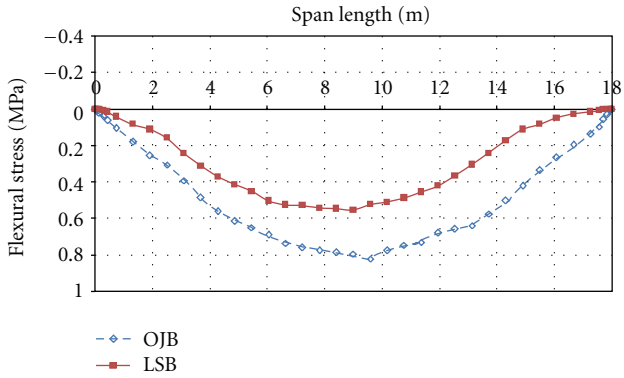

Figure 11: Flexural stresses for bottom elements of 2nd girder in 2nd span (S2G2).

3.7. Stresses in Bridge Decks. In bridge decks, the maximum and minimum transverse, longitudinal, and shear stresses were found in the first deck of the open joint bridge or the link slab bridge, since the load was applied on the first span of the bridge. The use of link slab reduced the bridge deck stresses. The transverse stresses were reduced by more than 13%, the longitudinal stresses were reduced by more than 36%, and the shear stresses were reduced by more than 43%. Based on these results, the use of the link slab will improve the performance of the bridge decks.

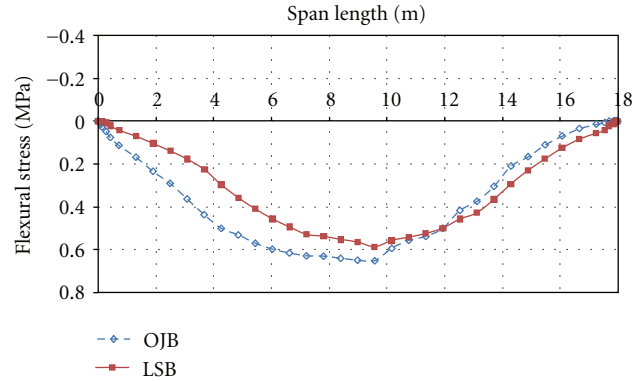

Figure 12: Flexural atresses for bottom elements of 2nd girder in 3rd span (S3G2).

3.8. Stresses in Link Slabs. The maximum and minimum transverse, longitudinal, and shear stresses in two link slabs were shown in Table 3. Slabs 1 and 2 were joined by link slab 1, and slabs 2 and 3 were joined by link slab 2. The stresses were higher in link slab 1 than those in the link slab 2 because the truck was placed on the first span of the bridge. Maximum and minimum stresses were either at the top surface or at the bottom surface of the link slab.

The longitudinal stresses along the depth or thickness of the link slab 1 for the bottom element and at the top element were −1.01 MPa (−146.7 psi) and 2.29 MPa (332.8 psi), respectively. The longitudinal stresses along the depth for the bottom element and at the top element of the link slab 2 were −0.20 MPa (−28.4 psi) and 1.05 MPa (151.9 psi), respectively. The longitudinal stresses varied from compression to tension from the bottom to the top elements of both link slabs. The maximum longitudinal stresses along the length of the link slabs for the top elements were 1.21 MPa (176.1 psi) and 0.62 MPa (89.6 psi) for link slabs 1 and 2, respectively. Along the length of the link slab, all top elements for both link slabs were in tension. The maximum and minimum longitudinal stresses were higher in the link slab 1 than those in the link slab 2 because the truck load was placed in the first span of the bridge and the link slab 1 was connecting the span 1 and the span 2 decks of the bridge. The maximum longitudinal stresses along the length of the link slabs for the bottom elements were 0.29 MPa (−42.1 psi) and 0.02 MPa (2.6 psi) for link slabs 1 and 2,

respectively. Along the length of the link slab, the bottom elements of link slab 2 were in tension.

4. Conclusions

The ductility of the FRP grid material was utilized to accommodate bridge deck deformations imposed by girder deflection, concrete shrinkage, and temperature variations. It would also provide a cost-effective solution to a number of deterioration problems associated with bridge deck joints.

The structural behavior of two types of FRP-grid-reinforced concrete slabs was investigated. Scaled-up beam specimens simulating the actual deck joint were prepared and tested. The design concept of link slabs was then examined to form the basis of design for FRP grid link slabs. Improved design of FRP grid link slab/concrete deck slab interface was confirmed in the numerical analysis.

The results indicated that the technique would allow simultaneous achievement of structural need, lower flexural stiffness of the link slab approaching the behavior of a hinge, and durability need of the link slab. The overall investigation supports the contention that durable jointless concrete bridge decks may be designed and constructed with FRP grid link slabs. It is recommended that the link slab technique be used during new construction of bridge decks. Also, it is recommended that the advantages of using the FRP grid link slab technique in repair and retrofit of bridge decks are considered along with the amount of intrusive field work required to develop the required mechanical properties at the bridge deck joints. The Louisiana Transportation Research Center received funds from the federal highway administration through the Innovative Bridge Research and Development program to support the implementation of the use of FRP grid as link slab.

Acknowledgments

Support of this work was provided by Louisiana Transportation Research Center under research Project no. 06-2ST and State Project no. 736-99-1391. Also, the fiberglass grid used in this study was provided by the Fibergrate Composite Structures (http://www.fibergrate.com/). The contents of this study reflect the views of the authors who are responsible for the facts and the accuracy of the data presented herein. The contents do not necessarily reflect the official views or policies of the Louisiana Department of Transportation, or the Louisiana Transportation Research Center, or the Fibergrate Composite Structures. This paper does not constitute a standard, specification, or regulation.

References

[1] A. Saber, F. Roberts, J. Toups, and W. Alaywan, "Effects of continuity diaphragm for skewed continuous span precast prestressed concrete girder bridges," *The Precast/Prestressed Concrete Institute Journa*, vol. 52, no. 2, pp. 108–114, 2007.

[2] A. Saber, J. Toups, and W. Alaywan, "Effects of continuity on load transfer in prestressed concrete skewed bridges," in *Proceedings of the 3rd International Structural Engineering and Construction*, 2005.

[3] A. Saber, "'Failure Behavior of RC T-Beams retrofitted with Carbon FRP Sheets.' Creative Systems in Structural and Construction Engineering," in *Proceeding of the 1st International Structural Engineering and Construction*, Honolulu, Hawaii, USA, 2001.

[4] K. P. Dutta, M. D. Bailey, R. J. Hayes, W. D. Jensen, and W. S. Tsai, "Composite grids for reinforcement of concrete structures," *Construction Productivity Advancement Research Program*, Final report, 1998.

[5] American Concrete Institute, "Building Code Requirements for Structural Concrete," ACI 318-05.

[6] American Concrete Institute, "Report on fiber reinforced plastic, reinforcement for concrete structure," ACI 440R, 2002.

[7] A. Saber, J. Toups, and A. Tayebi, "Continuity diaphragms for aashto type II girders," in *Proceedings of the 2nd International Structural Engineering and Construction*, Rome, Italy, August 2003.

[8] P. Zia, C. Alp., and K. E. S. Adel, *Jointless Bridge Decks*, North Carolina Department of Transportation, 1995.

[9] A. Saber, F. Roberts, X. Zhou, and W. R. Alaywan, "Impact of higher truck loads on remaining safe life of Louisiana bridge decks," in *Proceedings of the 9th International Conference, Applications of Advanced Technology in Transportation*, Chicago, Ill, USA, August 2006.

[10] American Association of State and Highway Transportation Officials, *LRFD Bridge Design Specifications*, U.S. Customary Units, 3rd edition, 2004.